Eur Biophys J (1986) 13:219–233

European Biophysics Journal

The human erythrocyte membrane skeleton may be an ionic gel

II. Numerical analyses of cell shapes and shape transformations

B. T. Stokke*, A. Mikkelsen, and A. Elgsaeter

Division of Biophysics, University of Trondheim, N-7034 Trondheim – NTH, Norway

Received June 17, 1985/ Accepted October 15, 1985

Abstract. In the first paper in this series (Stokke et al. Eur Biophys J 1986, 13:203–218) we developed the general theory of the mechanochemical properties and the elastic free energy of the protein gel – lipid bilayer membrane model. Here we report on an extensive numerical analysis of the human erythrocyte shapes and shape transformations predicted by this new cell membrane model. We have calculated the total elastic free energy of deformation of four different cell shape classes: disc-shaped cells, cup-shaped cells, crenated cells, and cells with membrane invaginations. We find that which of these shape classes is favoured depends strongly on the spectrin gel osmotic tension, Π_{Gu}, and the surface tensions, Π_{Eu} and Π_{Pu}, of the extracellular and protoplasmic halves of the membrane lipid bilayer, respectively. For constant ratio $\Pi_{Eu}/\Pi_{Pu} > 0$ large negative or positive values of Π_{Gu} favour respectively the crenated and invaginated cell shape classes. For small absolute values of Π_{Gu}, Π_{Eu}, and Π_{Pu}, biconcave or cup-shaped cells are the stable ones. Our numerical analysis shows that the higher the membrane skeleton compressibility is, the smaller are the values of Π_{Gu} needed to induce cell shape transformation. We find that the stable and metastable shapes of discocytes and stomatocytes generally depend both on the shape of the stressfree membrane skeleton and the membrane skeleton compressibility.

Key words: Erythrocyte, protein gel, cell shape, cell membrane model, membrane skeleton

Introduction

The beauty and simple geometry of human erythrocyte shapes have long intrigued biophysicists, cell biologists and others. Numerous studies suggest that spectrin plays a crucial role in determining the mechanical properties and stable shapes of erythrocytes by forming a macromolecular meshwork on the cytoplasmic side of the cell membrane. This has been the topic of several recent reviews (Branton et al. 1981; Bennett 1982; Cohen 1983; Gratzer 1983; Sheetz 1983). Over the years, numerous attempts have been made to elucidate the physical and mathematical basis for the characteristic erythrocyte shapes (Fung and Tong 1968; Canham 1970; Bull 1972; Skalak et al. 1973; Brailsford and Bull 1973; Evans 1973, 1974; Sheetz and Singer 1974; Deuling and Helfrich 1976; Evans and Hochmuth 1977, 1978; Evans and Skalak 1979; Brailsford et al. 1980a, b; Markin 1981). But, despite a wealth of biochemical data on the isolated components of the spectrin network, no unifying molecular cell membrane model relating all of these features to cell shape and shape transformations has yet been put forward.

In the first paper in this series (Stokke et al. 1986) we derived the general theory of the mechanochemical properties and the elastic free energy of a new cell membrane model which we named the protein gel – lipid bilayer membrane model. This model gives a coherent molecular and theoretical basis for the human erythrocyte mechanochemical properties. Here we present the results of an extensive numerical analysis of erythrocyte membrane skeleton density distributions, shapes, and shape transformations assuming that the spectrin network constitutes an ionic gel (swollen ionic elastomer) and that the general theory of our new membrane model is applicable to the erythrocyte membrane. Our findings indicate that all the commonly observed human erythrocyte shape and shape transformations can be accounted for by the new model.

Erythrocyte membrane elastic free energy

We limit our numerical analysis of erythrocyte total elastic free energy to cell shapes Ψ_d with global or

* To whom offprint requests should be sent

local rotational symmetry. All the numerical analyses we present are therefore based on the notation and mathematical formulas described by Stokke et al. (1986). To facilitate the presentation and discussion of our numerical analysis it is useful to introduce dimensionless quantities in the elastic free energy master equation of the protein gel – lipid bilayer membrane model:

$$\begin{aligned}\Delta F'_{\text{tot}} &\equiv \Delta F_{\text{tot}}/(\tfrac{1}{2} G\, 4\pi R_0^2)\\ &= I'_1 + (K_{Gu}/G)\, I'_3 + [B_L/(G R_0^2)]\, I'_4\\ &+ \begin{cases} 2\,(\Pi_{Gu}/G)\, d'\, \partial(\Delta A')/\partial z' & \text{when } \Pi_{Gu} \neq 0\\ 2\,(\Pi_{Pu}/G)\, b'\, \partial(\Delta A')/\partial z' & \text{when } \Pi_{Gu} = 0 \end{cases}\\ &+ \tfrac{1}{2}(K_{Lu}/G)\,(\Delta A'_G + (a' + 3b'/2)\,\partial(\Delta A')/\partial z')^2/A'_{Eu}\\ &+ \tfrac{1}{2}(K_{Lu}/G)\,(\Delta A'_G + (a' + \tfrac{1}{2}b')\,\partial(\Delta A')/\partial z')^2/A'_{Pu}\,, \end{aligned} \tag{1}$$

where

$$I'_1 \equiv [1/(4\pi R_0^2)] \int_{\Omega_{Gu}} \int (l_x/l_u - l_y/l_u)\, d^2 r \geq 0 \tag{2}$$

$$I'_3 \equiv [1/(4\pi R_0^2)] \int_{\Omega_{Gu}} \int (1 - l_x\, l_y/l_u^2)^2\, d^2 r \geq 0 \tag{3}$$

$$I'_4 \equiv [1/(4\pi R_0^2)] \cdot \int_{\Omega_{Lu}} \int [(R_1/R_0)^{-2} + (R_2/R_0)^{-2}]\, d^2 r \geq 2 \tag{4}$$

$$a' \equiv a/R_0 \tag{5}$$

$$b' \equiv b/R_0 \tag{6}$$

$$d' \equiv a' + b'[\tfrac{1}{2} + (1 + \Pi_{Pu}/\Pi_{Eu})^{-1}] \tag{7}$$

$$\Delta A' \equiv \Delta A/(4\pi R_0^2) \tag{8}$$

$$z' \equiv z/R_0\,. \tag{9}$$

G is the elastic shear modulus of the membrane skeleton. The cell surface area equals $4\pi R_0^2$. Since $G \approx 7 \times 10^{-3}$ dyne/cm and $R_0 \sim 3.5\,\mu$m for erythrocytes, $\frac{1}{2} G\, 4\pi R_0^2 \approx 3 \times 10^{-14}$ Nm $\approx 10^5$ kT at room temperature where k is the Boltzmann constant and T is the absolute temperature. Ω_{Gu} is the gel surface of cell shape Ψ_u. Π_{Gu} is the osmotic tension of the gel of Ψ_u. K_{Gu} is the gel modulus of area compression. B_L is the lipid bilayer elastic bending modulus. Π_{Eu} and Π_{Pu} are the surface tension of the extracellular and the protoplasmic half of the lipid bilayer of Ψ_u. a is the distance from the middle of the gel at the points where the gel is attached to the membrane integral proteins to the protoplasmic surface of the membrane lipid bilayer. b is the thickness of each half of the lipid bilayer. A_{Eu} and A_{Pu} are the total surface area of the midplane of the extracellular and protoplasmic halves of the lipid bilayer of Ψ_u. ΔA_G is the change in gel surface area resulting from cell shape change $\Psi_u \rightarrow \Psi_d$. ΔA is the change in area of a plane located a distance z from the gel when $\Psi_u \rightarrow \Psi_d$. K_{Lu} is the modulus of area compression of the lipid bilayer of Ψ_u. Ω_{Lu} is the bilayer midplane of Ψ_u. The equilibrium radius of curvature of the two halves of the lipid bilayer have been assumed to be infinite. R_1 and R_2 are the principal radii of curvature of Ω_{Lu}. For a detailed description of the symbols see Stokke et al. (1986).

Cell shape parameterization

Several different strategies can be followed to determine the stable erythrocyte shapes predicted by the protein gel – lipid bilayer cell membrane model. The strategy which generally leads to the most accurate description of the predicted stable shape for a given set of conditions involves expressing the cell radius $r_d(s_d)$ of cell shape Ψ_d (Stokke et al. 1986) as a sum of mutually orthogonal functions which make up a complete set. The disadvantage of this method is that the change in overall geometry, resulting from a change in one or more of the coefficients of the various orthogonal functions is generally complex. Further, it is generally not obvious which coefficients should be changed and by how much, in order to change a certain geometric detail without simultaneously changing the rest of the cell shape. This latter problem is eliminated if the cell shape parameterization is instead based on a geometric construction so that every parameter has a simple geometric meaning. The disadvantage of this geometric parameterization is that it can only generate a limited family of different cell shapes, the stable cell shape may not be contained among the cell shapes generated by the chosen parameterization and transformation from one shape class to another may not be geometrically possible by the chosen cell shape parameterization. But, using such a parameterization one will normally obtain the particular cell shape among all the ones generated by the parameterization which comes closest to the stable cell shape or one of the metastable shapes. We have used the geometric parameterization strategy in part because it provides the easiest approach to independently changing one geometric parameter at a time and in part because it facilitates separation of cell shapes into classes with certain characteristic shape features in common.

The cell shape parameterization of the four main cell shape classes displayed by human erythrocytes is based on the geometric construction shown in Fig. 1. The first two of these classes have global cell shape rotational symmetry whereas the last two only have approximate local rotational symmetry. Cell shape class I consists of a continuum of cell shapes ranging from oblate to biconcave discs with the axis of global rotational symmetry perpendicular to a plane of mirror symmetry (Fig. 1A). Class II consists of cup-shaped cells (Fig. 1B). Class III consists of

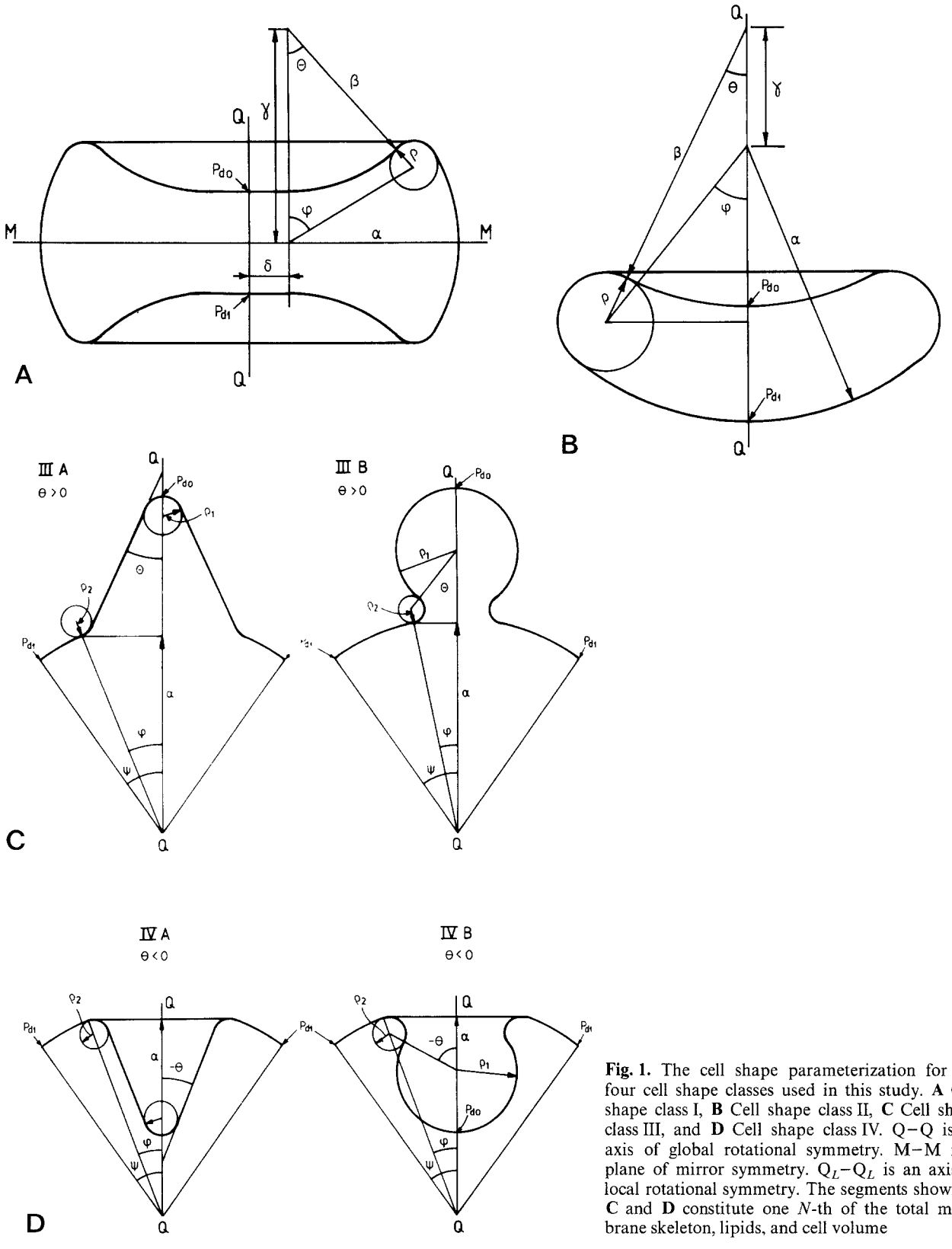

Fig. 1. The cell shape parameterization for the four cell shape classes used in this study. **A** Cell shape class I, **B** Cell shape class II, **C** Cell shape class III, and **D** Cell shape class IV. Q−Q is an axis of global rotational symmetry. M−M is a plane of mirror symmetry. Q_L−Q_L is an axis of local rotational symmetry. The segments shown in **C** and **D** constitute one N-th of the total membrane skeleton, lipids, and cell volume

Table 1. Characteristic parameters of membrane skeleton stress free shapes

Cell shape	Ψ_{us}	Ψ_{u3}	Ψ_{u4}	Ψ_{u6}	Ψ_{u10}
$r'_u(P'_u/2)$	1	1.033	1.118	1.208	1.285
P'_u	π	3.098	2.981	2.898	2.854
ξ_u	1	0.998	0.959	0.847	0.660
$\delta A'_u/\delta z'$	−2	−2.00	−2.02	−2.06	−2.11

cells with a variable number of identical exocytic blebbs or spikes (Fig. 1C). Class IV consists of cells with a variable number of identical pointed or blebb-like invaginations (Fig. 1D). The mathematical expression for the cell shape radius $r_d(s_d)$ and the volume and surface area for these cell shape classes are given elsewhere (Stokke 1985).

We have chosen to study the effect of varying Ψ_u partly because shape Ψ_u of human erythrocytes is not yet known (Stokke et al. 1986) and partly in order to study the effect of assuming various shapes Ψ_u. We use a simple parameterization for Ψ_u that can generate discoidal as well as spherical Ψ_u, all with the same surface area $4\pi R_0^2$ (Table 1). This parameterization has only one free variable, n, and the larger n is, the thinner and flatter the discoids become. We refer to the discoid corresponding to a certain value of n as Ψ_{un}. All Ψ_{un}'s have a plane of mirror symmetry. Note that parameter n does not have to be an integer. Spherical Ψ_u we denote Ψ_{us}. We call the volume of Ψ_d divided by $(4\pi/3)R_0^3$ the relative volume of Ψ_d and designate this relative volume by the symbol ξ_d.

Numerical analysis

All our numerical analysis is based on computer minimalization of $\Delta F'_{\text{tot}}$ including some or all the terms of Eq. (1). Integrals I'_1 and I'_3 were calculated using the approach described by Stokke et al. (1986) and expressing the change in $s_u^+(s_d)$ due to gel relaxation by means of the Fourier expansion:

$$s_u^+(s_d) - P_u s_d/P_d = P_u \sum_{m=1}^{\infty} C_m \sin(\pi m s_d/P_d), \qquad (10)$$

where C_m are the Fourier coefficients. For all values of C_m this expression automatically satisfies the boundary conditions $s_u^+(0) = 0$ and $s_u^+(P_d) = P_u$. Since the same gel latitudinal line cannot be found at more than one distance s_d from pole P_{d0}, the function $s_u^+(s_d)$ must also satisfy the conditions $ds_u^+(s_d)/ds_d > 0$. The values of I'_1 and I'_3 for unrelaxed gels can be obtained by setting all C_m equal to zero in Eq. (10).

The basic strategy has been the same for all our numerical calculations of erythrocyte membrane elastic free energy: First we chose numerical values for all except two of the freely variable geometric parameters of the cell shape parameterization being used. Then we determined the remaining freely variable geometric parameters using the requirement that the gel surface of Ψ_u equals $4\pi R_0^2$, the relative gel surface area of Ψ_d, ζ_d, equals $1+\Delta A_G/(4\pi R_0^2)$, and the relative gel volume ξ_d has the selected values. This we achieved by solving simultaneously the equations expressing these constraints using computer routine C05NAF of the Numerical Algorithm Group (NAG Ltd., Oxford, England) Mark 8 library routines. The numerical integrations needed to calculate $\Delta F'_{\text{tot}}$ were performed using function D01BAF of the NAG library. The minimalization of $\Delta F'_{\text{tot}}$ with respect to the Fourier coefficients C_m was performed using NAG routine E04JAF. We performed these minimalizations allowing 3–8 Fourier coefficients to vary and setting all the other Fourier coefficients equal to zero. NAG routine E04UAF was used to minimize $\Delta F'_{\text{tot}}$ when both the Fourier coefficients and the remaining freely variable geometric parameters of the shape parameterization were allowed to vary during the minimalization. When the geometric parameters are included in the minimalization process, it is important to note that the geometric parameters must always satisfy certain inequality and range constraints to ensure that the obtained minimum corresponds to a physical solution. We performed all the numerical calculations involving the NAG library using the UNIVAC 1100/62 computer at RUNIT computing centre at the University of Trondheim.

Spectrin gel relaxation

One important feature of the protein gel – lipid bilayer membrane model that sets it apart from all other membrane models used to analyze erythrocyte shapes, is that the membrane skeleton of our model may slide in the plane of the lipid bilayer and change its density distribution as the cell shape is changed. Figure 2 shows the contribution $\Delta F'_1 = I'_1 + (K_{Gu}/G) I'_3$ to $\Delta F'_{\text{tot}}$ from the gel shear deformation and non-uniform gel compression for various discoidal cell shapes for both unrelaxed and relaxed gels when $K_{Gu}/G = 5$. Relaxation of the spectrin gel generally leads to reduction of $\Delta F'_1$. The numerical results also show that the cell shape which yields the minimum contribution to $\Delta F'_{\text{tot}}$ is generally not the same for relaxed and unrelaxed spectrin gel (Fig. 2). Stokke et al. (1986) showed analytically that $\Delta F'_1$ of the relaxed membrane gel of a cell with global axial symmetry equals zero for all cell shapes with $G = 0$

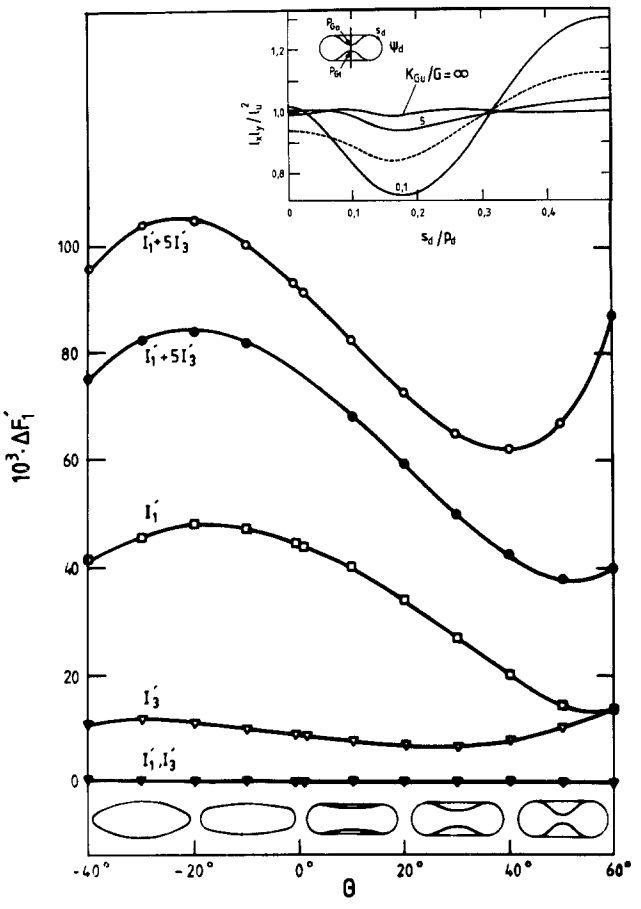

Fig. 2. The computed gel elastic free energy $\Delta F_1' = I_1' + (K_{Gu}/G) I_3'$ for some cell shapes of class I with $\xi_d = 0.7$, $\varphi = 90°$, $\delta' = 0$, and some selected values of θ. Smooth curves are drawn through the data points. The examples illustrate the reduction in $\Delta F_1'$ resulting from gel relaxation: Free energy, $\Delta F_1' = I_1' + 5I_3'$, for unrelaxed (○) and relaxed gel (●). When the gel elastic shear modulus, G, equals zero, $\Delta F_1' = I_3'$. When the gel modulus of area compression, K_{Gu}, equals zero, $\Delta F_1' = I_1'$. For unrelaxed gel I_1' (□) and I_3' (▽) are cell shape dependent, but for relaxed gel, I_1' and I_3' (▼) both equal zero for all cell shapes when the gel relaxation is carried out for $K_{Gu} = 0$ and $G = 0$ respectively. The change in spectrin gel density distribution associated with changing the cell shape from spherical to discoid shape Ψ_d of class I with $\xi_d = 0.7$, $\varphi = 90°$, $\theta = 50°$, and $\delta' = 0$ when Ψ_u is spherical (inset). For non-spherical Ψ_d the gel density of the unrelaxed (– – –) and relaxed (——) spectrin gel varies with the distance s_d from the gel pole (measured along the gel surface). The gel poles are the points, P_{G0} and P_{G1}, where the axis of rotational symmetry passes through the gel surface. P_d is the pole-to-pole distance measured along the gel surface

or $K_{Gu} = 0$. Our numerical analysis of the effect of relaxing the gel so as to minimize I_1' alone or I_3' alone for various cell shapes confirms this conclusion (Fig. 2). The density distribution generally changes as a result of gel relaxation when $K_{Gu}/G < 10$. How large the change is for a selected cell shape depends sharply on K_{Gu}/G (Fig. 2 inset). The reason why the numerically predicted gel density distribution is not perfectly uniform for $K_{Gu}/G = \infty$ is that only a limited number of terms were used in the Fourier expansion of the gel density distribution. As the number of Fourier terms is increased the numerically predicted gel density for $K_{Gu}/G = \infty$ becomes more and more uniform. Stokke et al. (1986) showed analytically that for $K_{Gu}/G = 0$ there is a continuum of gel density distributions which yields zero $\Delta F_1'$ for any shape with global axial shape symmetry. Our numerical analysis yields the density distribution from this continuum which can be best approximated by the number of Fourier terms used.

If all the erythrocyte intramembrane particles were attached to, and randomly distributed over, the spectrin network, then the intramembrane particle density would reflect the spectrin gel density. If so, a careful analysis of the intramembrane particle density distribution for known Ψ_u could be used to obtain information about K_{Gu}/G, and vice versa.

The effect of lipid bilayer bending resistance on cell shape

The third term of Eq. (1) represents the contribution from the lipid bilayer local bending resistance to the membrane total elastic free energy. The elastic free energy increases sharply as the radius of curvature is reduced. The lipid bilayer bending resistance tends therefore to make the favoured cell shapes smoother than they otherwise might have been. Figure 3 shows examples of elastic free energy versus cell shape when one geometric parameter of the cell shape parameterization of disc-shaped cells is varied. The numerical analyses were performed with relaxed gel, but for simplicity, only the first three terms of $\Delta F_{\text{tot}}'$ (Eq. (1)) were included in the energy calculations. For small values of $B_L/(GR_0^2)$ (Fig. 3A and C) and large values of K_{Gu}/G the favoured cell shapes are, as expected, the shapes contained in the cell shape class studied which correspond to no gel deformation (Fig. 8, Stokke et al. 1986). The favoured cell shape becomes more rounded as $B_L/(GR_0^2)$ is increeased (Fig. 3B and D). Figure 3 also shows that the lipid bilayer bending resistance's influence on the favoured cell shape for a selected value of $B_L/(GR_0^2)$ increases as K_{Gu}/G is decreased. When $K_{Gu}/G = \infty$ the gel is incompressible and the results presented correspond to those of Brailsford et al. (1976).

The trilayer couple term

The fourth term of Eq. (1) is a mathematical expression for a trilayer analogue of the bilayer couple hypothesis (Sheetz and Singer 1974). This term only depends on Ψ_d through the derivative $\partial(\Delta A')/\partial z'$

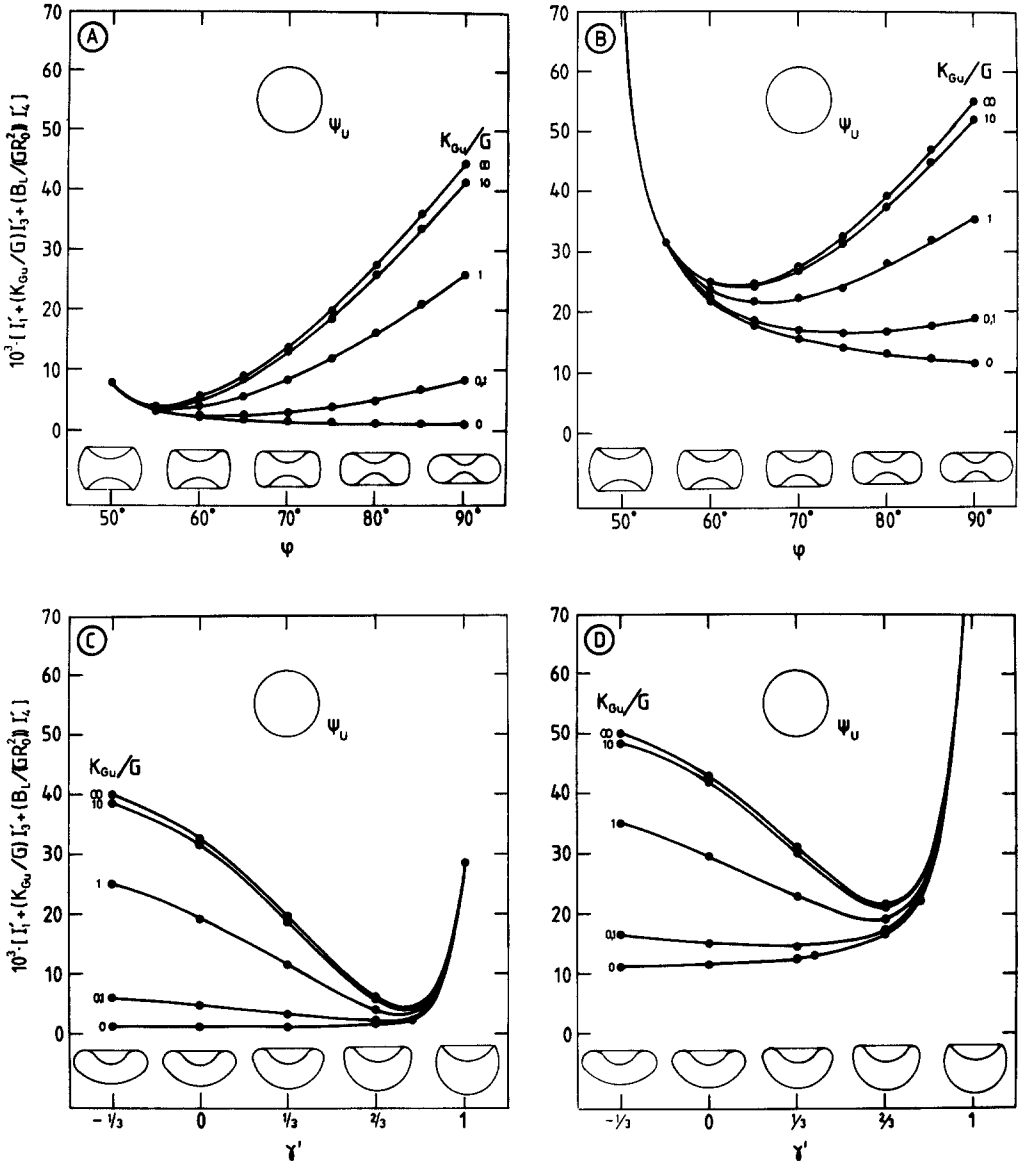

Fig. 3. Examples illustrating the effect of lipid bilayer bending resistance on the total cell membrane elastic free energy for some cell shapes of class I with $\xi_d = 0.7$, $\theta = 50°$, and $\delta' = 0$ (**A** and **B**) and some cell shapes of class II with $\xi_d = 0.7$ and $\theta = 60°$ (**C** and **D**) when $B_L/(GR_0^2) = 10^{-4}$ (**A** and **C**) and $B_L/(GR_0^2) = 10^{-3}$ (**B** and **D**). The gel free energy $\Delta F_1'$ has been calculated assuming $\Psi_u = \Psi_{us}$ and that the gel is relaxed

$\equiv \partial A_d'/\partial z' - \partial A_u'/\partial z'$. For spherical Ψ_u the derivative $\partial A_u'/\partial z' = -2.00$. As Ψ_u becomes more and more disc-shaped $\partial A_u'/\partial z'$ changes relatively little and for Ψ_{u10} $\partial A_u'/\partial z' = -2.11$ (Table 1). Figure 4 shows $\partial A_d'/\partial z'$ for various geometric parameters and relative cell volume, ξ_d, for respectively discocytes (Fig. 4A), stomatocytes (Fig. 4B), echinocytes (Fig. 4C), and invaginated cell shapes (Fig. 4D). The results show that $\partial(\Delta A')/\partial z'$ is negative for crenated, but positive for invaginated cells. $\partial(\Delta A')/\partial z'$ for discocytes and stomatocytes may be positive or negative, but is generally much smaller in magnitude than for the other shape classes. When Π_{Eu} and Π_{Pu} have the same sign, crenated shapes are favoured for negative Π_{Gu} whereas invaginated cell shapes are favoured for positive Π_{Gu}. Among cup-shapes, shallow cups are favoured for negative Π_{Gu} and deep cup-shapes with a narrow mouth for positive Π_{Gu}. It is important to note that the shape favoured by the trilayer couple term alone depends only on the sign and not on the magnitude of Π_{Gu}. This means that even though the trilayer couple term incorporates an important mechanism for cell shape transformation, it is alone unable to predict quantitatively the commonly observed cup-shapes. The trilayer couple term for example predicts that cell shapes with multiple invaginations rather than cup-shapes is preferred for all values of $\Pi_{Gu} > 0$ when $\Pi_{Pu}/\Pi_{Eu} > 0$.

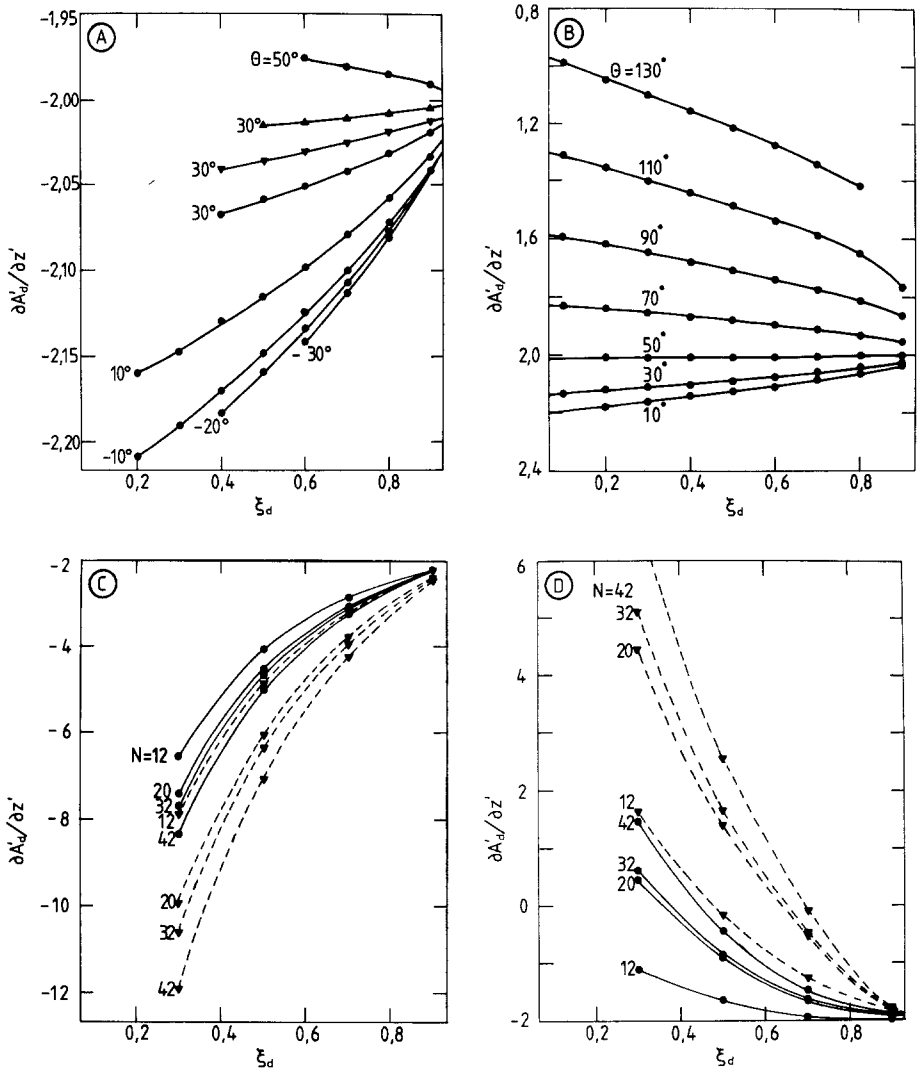

Fig. 4. The derivative $\partial A'_d/\partial z'$ versus relative cell volume, ξ_d. **A** cell shape class I with $\delta' = 0$ and $\varphi = 90°$ (●), $\varphi = 80°$ (▼), and $\varphi = 70°$ (▲), **B** cell shape class II with $\gamma' = 0$, **C** cell shape class IIIA with $\varphi/\varphi_{max} = 1$ and $\varrho'_1 = \varrho'_2 = 0.03$ (●) and $\varphi/\varphi_{max} = 0.6$ and $\varrho'_1 = \varrho'_2 = 0.03$ (▼), and **D** cell shape class IVB with $\varphi/\varphi_{max} = 1$ and $\varrho'_1 = \varrho'_2 = 0.03$ (●), and $\varphi/\varphi_{max} = 0.6$ and $\varrho'_1 = \varrho'_2 = 0.03$ (▼)

The effect of lipid bilayer modulus of area compression on cell shape

The cell shape change $\Psi_u \rightarrow \Psi_d$ will generally change the surface areas of the two monolayers of the membrane lipid bilayer and thus lead to changes in the tension of the two monolayers of the bilayer. This is the physical basis for the two last terms of Eq. (1). To estimate the influence of these terms on the cell shape, an estimate of ΔA_G is needed. For the erythrocyte membrane there will always be a plane within the membrane that maintain constant surface area during the cell shape change $\Psi_u \rightarrow \Psi_d$ (Stokke et al. 1986) which means that $\Delta A'_G \leq (a' + 2b')\,\partial(\Delta A')/\partial z'$. Assuming $K_{Lu} \approx 10-100$ dyne/cm, $a \approx 1$ nm, $b \approx 2$ nm, and $R_0 \approx 3.3$ μm, this shows that the sum of the last two terms in Eq. (1) must be positive and less than $(10^{-2} - 10^{-1})\,(\partial(\Delta A')/\partial z')^2$. These terms of Eq. (1) therefore always favour discocytes and stomatocytes rather than echinocytes and invaginated cell shapes. However, these terms have negligible effect on the favoured shapes of discocytes and stomatocytes.

Discocytes

The discocyte cell shapes generated by the class I parameterization (Fig. 1A) range from biconvex to biconcave shapes all with a global axis of rotational symmetry perpendicular to a plane of mirror symmetry.

The contribution from $\Delta F'_1 = I'_1 + (K_{Gu}/G)\,I'_3$ to $\Delta F'_{tot}$ for some class I discocytes ranging from biconvex to biconcave and Ψ_u being spherical (Ψ_{us}) or

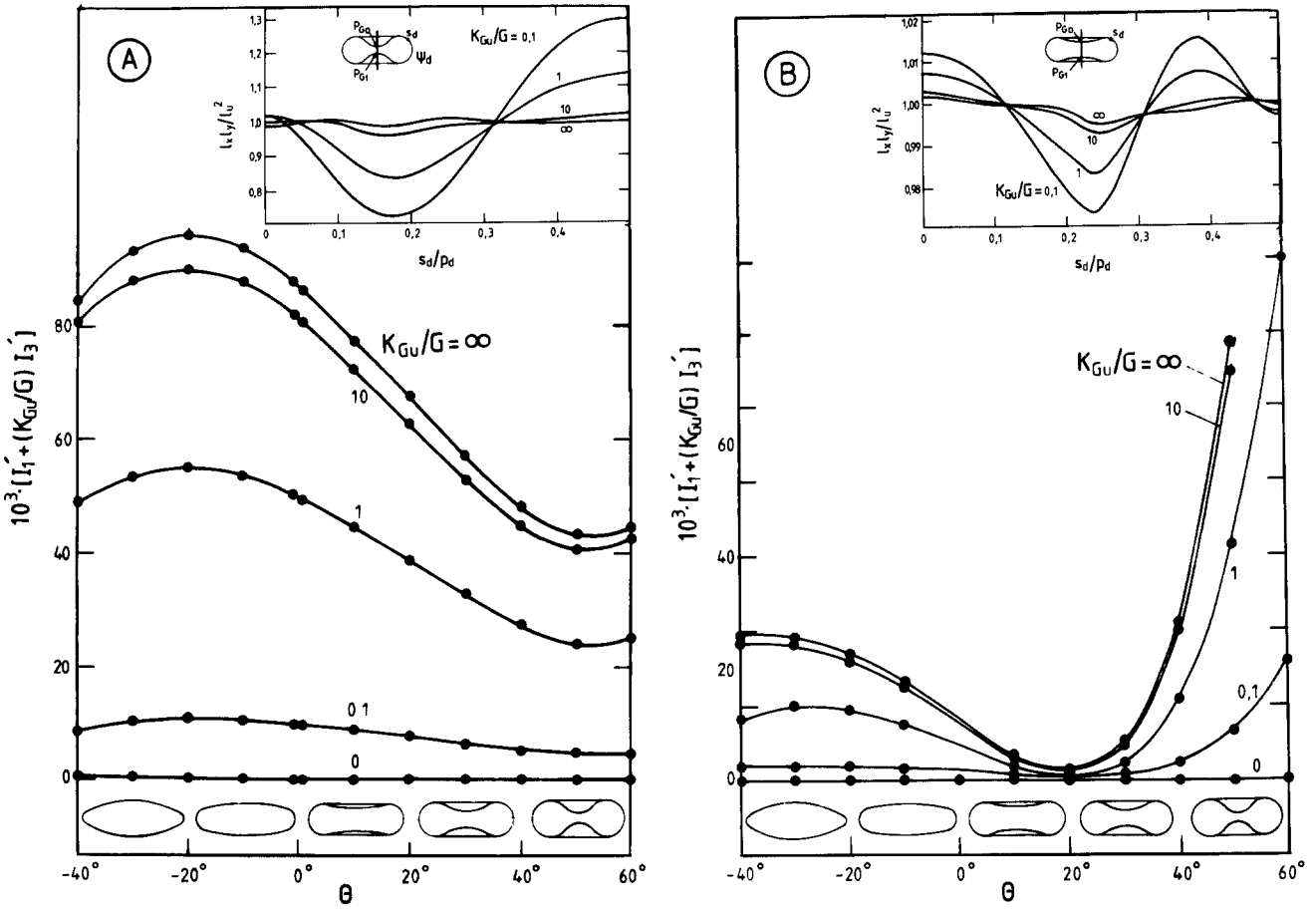

Fig. 5. The elastic free energy $\Delta F_1' = I_1' + (K_{Gu}/G)\, I_3'$ of the relaxed spectrin gel for some selected class I cell shapes with $\xi_d = 0.7$, $\varphi = 90°$, and $\delta' = 0$ for $\Psi_u = \Psi_{us}$ (**A**) and $\Psi_u = \Psi_{u6}$ (**B**). The gel relaxation and the corresponding gel elastic free energy calculated were carried out for $K_{Gu}/G = 0$, 0.1, 1, 10, and ∞, respectively. The relative spectrin gel density distribution versus distance s_d from the gel pole P_{G0} (measured along the surface) of the favoured cell shape of **A** and **B** (*insets*), were calculated for relaxed spectrin gel with $K_{Gu}/G = 0.1$, 1, 10, and ∞, respectively

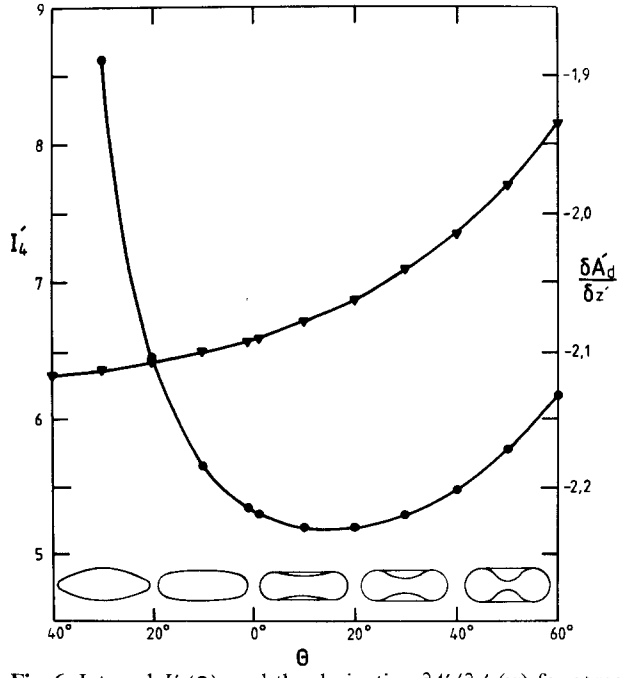

Fig. 6. Integral I_4' (●), and the derivative $\partial A_d'/\partial z'$ (▼) for some selected class I cell shapes with $\xi_d = 0.7$, $\varphi = 90°$, and $\delta' = 0$

disc-shaped (Ψ_{u6}), is shown in Fig. 5. In both cases $\Delta F_1'$ exhibits a distinct minimum for a single cell shape. The energy needed to change the shape a certain amount from the favoured shape to another similar shape (i.e., the cell shape stability) is in both cases sharply reduced as K_{Gu}/G is reduced. For the same value of K_{Gu}/G the stability of the favoured cell shape is sharply reduced as Ψ_u is changed from spherical to discoidal, and this is also true for the relative variation in spectrin gel density over the cell surface (Fig. 5 insets). When $\xi_d < \xi_u$ for Ψ_{u6} and Ψ_{u10} $\Delta F_1'$ favours biconcave cell shapes, but when $\xi_d > \xi_u$ biconvex cell shapes are favoured. Among disc shapes the lipid bilayer bending resistance favours biconcave cell shapes when $\xi_d < 0.8$ (Fig. 6). When Π_{Eu} and Π_{Pu} have the same sign, the trilayer couple term favours biconcave shapes with deep invaginations for positive Π_{Gu} and biconvex shapes for negative Π_{Gu}. The interplay of all these terms determines the detailed geometry of the favoured discocyte shape, which therefore can be expected to depend on the environmental conditions (Stokke et al. 1986).

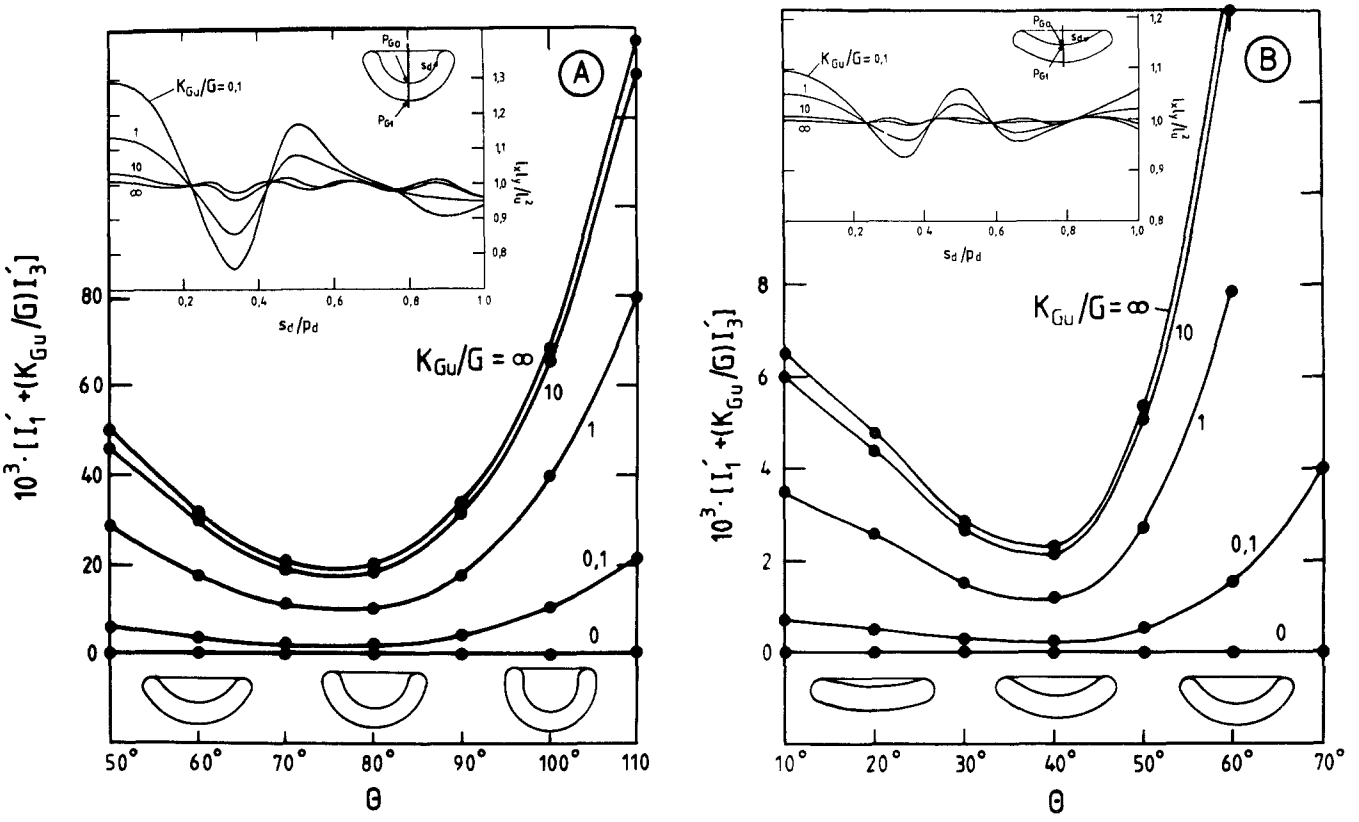

Fig. 7. The elastic free energy $\Delta F_1' = I_1' + (K_{Gu}/G)\, I_3'$ the relaxed spectrin gel for some selected class II cell shapes with $\xi_d = 0.5$ and $\gamma' = 0$ for $\Psi_u = \Psi_{us}$ (**A**) and $\Psi_u = \Psi_{u6}$ (**B**). The gel relaxations were carried out for $K_{Gu}/G = 0$, 0.1, 1, 10, and ∞, respectively. The relative spectrin gel density distribution versus distance s_d from the gel pole P_{G0} (measured along the surface) of the favoured cell shape of **A** and **B** (*insets*), were calculated for relaxed spectrin gel with $K_{Gu}/G = 0.1$, 1, 10, and ∞, respectively

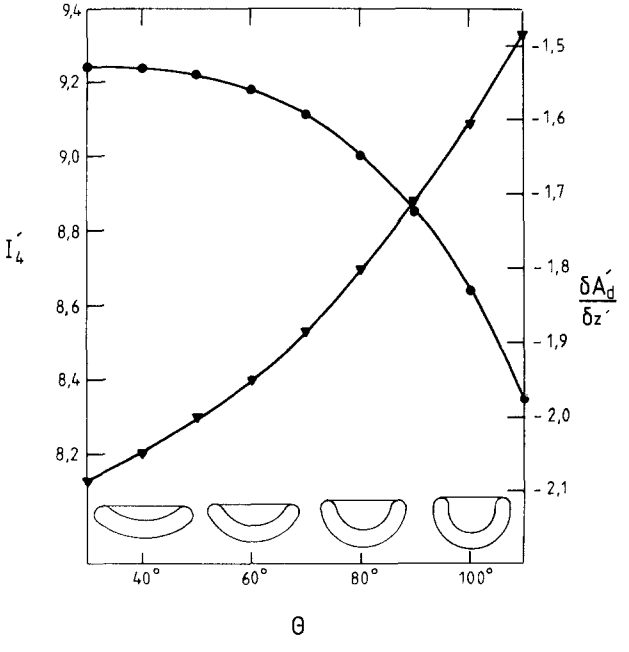

Fig. 8. Integral I_4' (●) and the derivative $\partial A_d'/\partial z'$ (▼) for some selected class II cell shapes with $\xi_d = 0.5$ and $\gamma' = 0$

Stomatocytes

The stomatocyte cell shapes generated by the class II parameterization (Fig. 1B) range from shallow cups to deeply invaginated shapes all with a global axis of rotational symmetry. The contributions from $\Delta F_1' = I_1' + (K_{Gu}/G)\, I_3'$ to $\Delta F_{tot}'$ for some class II cup-shaped cells ranging from shallow cups to deeply invaginated shapes and Ψ_u being spherical or disc-shaped (Ψ_{u6}) is shown in Fig. 7. In both cases $\Delta F_1'$ exhibits a distinct minimum for an intermediate cup-shape. The effects of Ψ_u and K_{Gu}/G on the stability of the favoured shape and spectrin gel density distribution (Fig. 7) are analogous to those for discocytes. The lipid bilayer bending resistance favours a deeply invaginated cup-shape (Fig. 8). When Π_{Eu} and Π_{Pu} have the same sign, the trilayer couple term favours deeply invaginated cupshapes for positive Π_{Gu} and shallow cupshapes for negative Π_{Gu}. The interplay of all these terms determines the detailed geometry of the favoured stomatocyte shape, which therefore can be expected to depend on the environmental conditions.

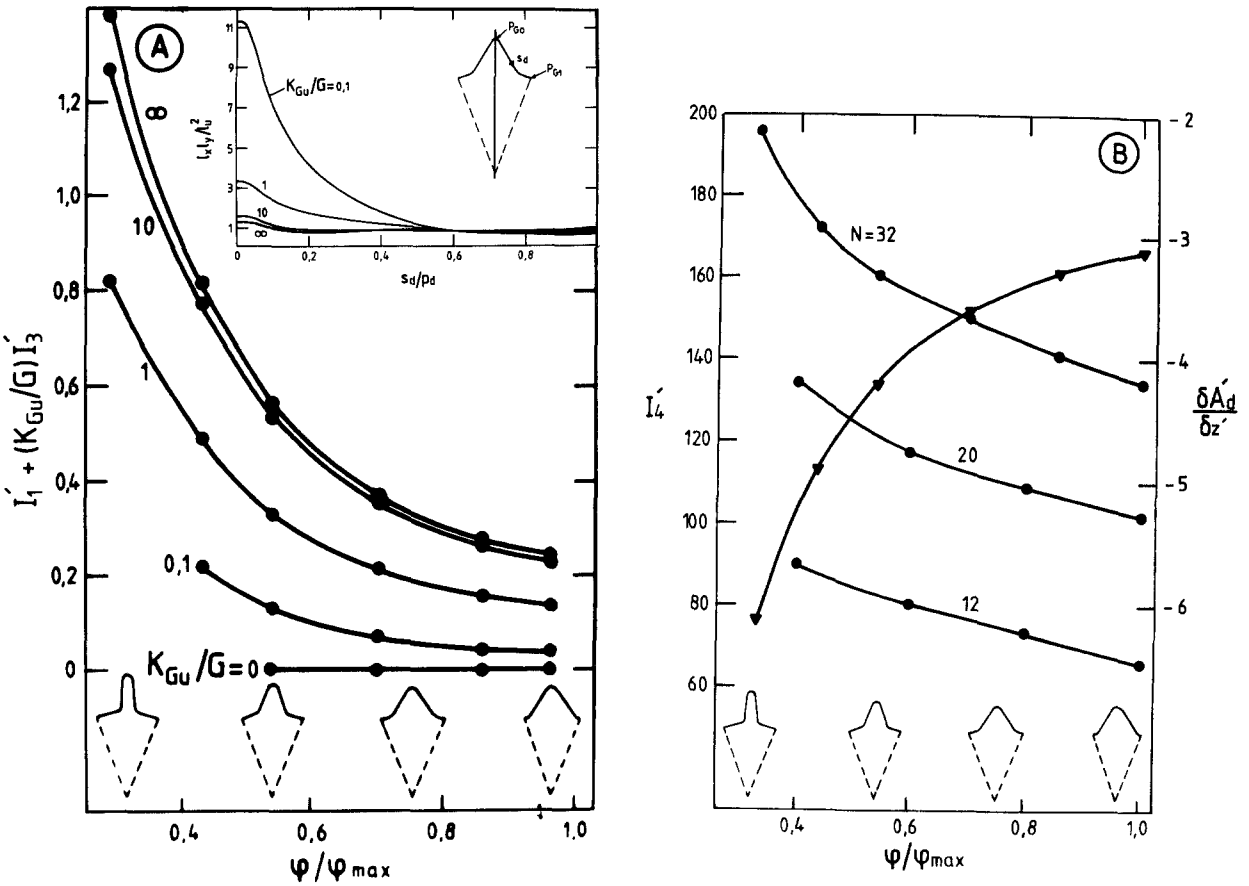

Fig. 9. The elastic free energy $\Delta F_1' = I_1' + (K_{Gu}/G)\, I_3'$ (●) of the relaxed spectrin gel (**A**), I_4' (●) and $\partial A_d'/\partial z'$ (▼) (**B**) for some selected class IIIA cell shapes with $\xi_d = 0.7$, $\varrho_1' = \varrho_2' = 0.03$, and $N = 32$. The elastic free energy calculation was carried out assuming $\Psi_u = \Psi_{us}$ and for $K_{Gu}/G = 0$, 0.1, 1, 10, and ∞, respectively. I_4' for cell shape class IIIA with $\xi_d = 0.7$, $\varrho_1' = \varrho_2' = 0.03$, and $N = 20$ and $N = 12$ are also included (**B**). Note that the shape illustrations are valid only for $N = 32$. The relative spectrin gel density distribution of class IIIA cell shape with $\xi_d = 0.7$, $\varrho_1' = \varrho_2' = 0.03$, $N = 32$, and $\varphi/\varphi_{max} = 0.7$ (*inset* **A**) were calculated assuming $\Psi_u = \Psi_{us}$ and for $K_{Gu}/G = 0$, 0.1, 1, 10, and ∞, rspectively

Echinocytes

The echinocyte cell shapes generated by the class III parameterization (Fig. 1C) consist of N identical segments each containing one N-th of the total cell volume, cell lipids, and spectrin network. Each segment has a local axis of rotational symmetry and contains one pointed or blebb-shaped protrusion. For $N > 10$ there are only two cases for which N identical segments can be packed together to yield a continuous surface. This is when the boundary symmetry of the segment surface is five-fold and $N = 12$, and when the symmetry is three-fold and $N = 20$. However, the number of spikes of echinocytes is most often neither 12 nor 20 and the spikes are normally irregularily packed on the cell surface (Sheetz et al. 1976). This suggests that the details of the packing of the protrusions are of minor importance to the cell membrane free energy and that the main contribution to $\Delta F_{tot}'$ stems from the geometric details of the protrusions themselves. The erythrocyte protrusions generally appear to have an axis of local rotational symmetry (Sheetz et al. 1976). There is therefore good reason for expecting that $\Delta F_{tot}'$ of cell shape class III with given N and protrusion shape, will not differ significantly from $\Delta F_{tot}'$ of a cell with continuous surface and the same spike number and spike shape. We assume that Ψ_u for each of the identical segments has an axis of rotational symmetry and equals one N-th of Ψ_{us}.

Figure 9 shows $\Delta F_1' = I_1' + (K_{Gu}/G)\, I_3'$, I_4' and $\partial A_d'/\partial z'$ for an echinocyte with 32 spikes, $\xi_d = 0.7$, and spike shapes gradually changing from spikes with a small base to those with as large a base as possible. For a given number of spikes $\Delta F_1'$ favours as large a spike base as possible (Fig. 9A). $\Delta F_1'$ for spikes with maximum base size decreases with increasing number of spikes. The lipid bilayer bending resistance also favours as large a base size as possible for the given spike number (Fig. 9B), but the free energy associated with the bending resistance increases sharply as the number of spikes is in-

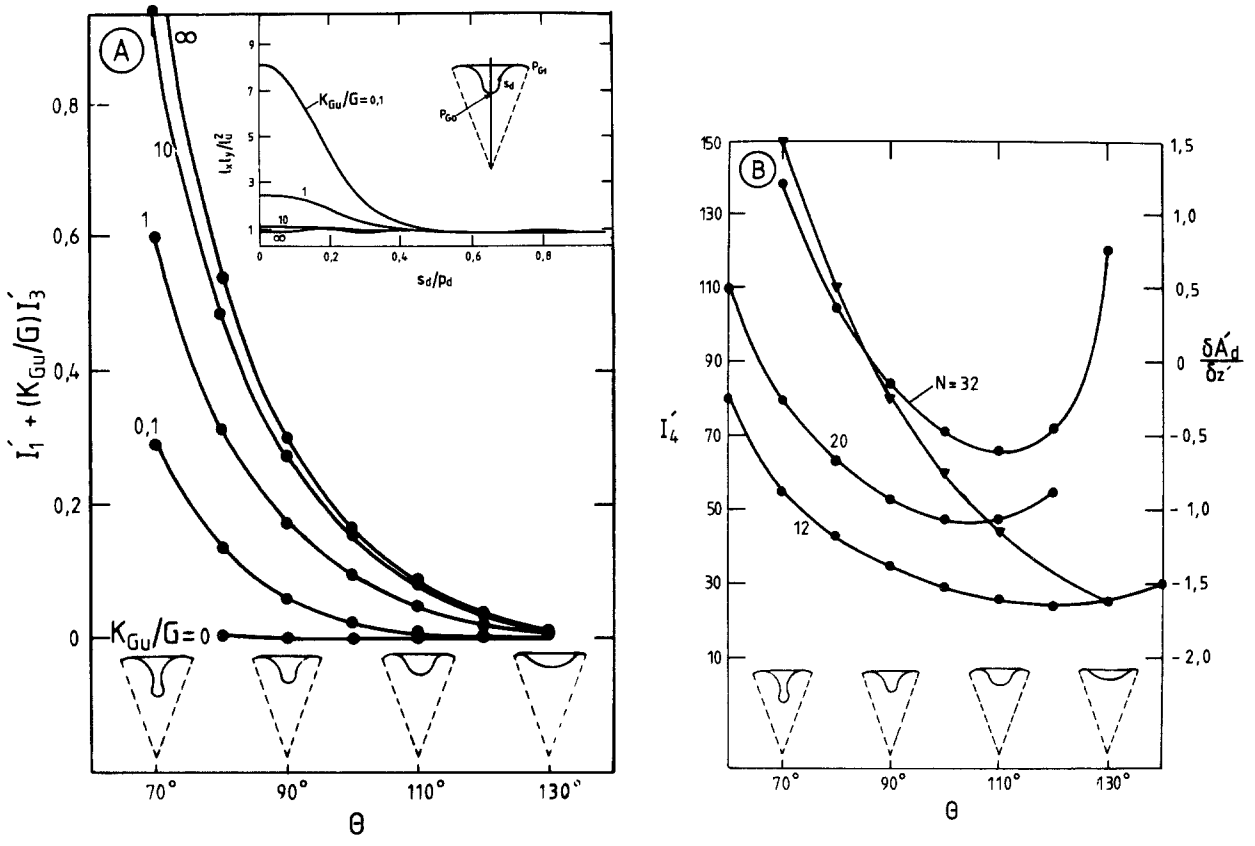

Fig. 10. The elastic free energy $\Delta F_1' = I_1' + (K_{Gu}/G)\, I_3'$ (●) of the relaxed spectrin gel (**A**), I_4' (●) and $\partial A_d'/\partial z'$ (▼) (**B**) for some selected class IVB cell shapes with $\xi_d = 0.7$, $\varphi/\varphi_{\max} = 0.95$ and $N = 32$. The elastic free energy calculation was carried out assuming $\Psi_u = \Psi_{us}$ and for $K_{Gu}/G = 0$, 0.1, 1, 10, and ∞, respectively. I_4' for cell shape class IVB with $\xi_d = 0.7$, $\varphi/\varphi_{\max} = 0.95$, and $N = 20$ and $N = 12$ are also included (**B**). Note that the shape illustrations are valid only for $N = 32$. The relative spectrin gel density distribution of class IVB cell shapes with $\xi_d = 0.7$, $\varphi/\varphi_{\max} = 0.95$, $N = 32$, and $\theta = 90°$ (*inset* **B**). The gel relaxations were carried out assuming $\Psi_u = \Psi_{us}$ and for $K_{Gu}/G = 0.1$, 1, 10, and ∞, respectively

creased. Because of the high value of $\Delta F_1'$ and high lipid bending energy (Fig. 9) echinocytes are only favoured for relatively large negative values of Π_{Gu} when Π_{Eu} and Π_{Pu} have the same sign. The trilayer couple term strongly favours pointed spikes rather than those with a broad base (Fig. 9B). The trilayer couple term increases with increasing spike number. Our numerical (Fig. 4C) analysis therefore predicts that as Π_{Gu} becomes more negative, the number of spikes of the favoured cell shape increases and the spikes tend to become more pointed. The analysis further predicts that the gel density will be highest at the tip of the spikes when $K_{Gu}/G \leq 10$, and that the density distribution (Fig. 9A inset) and the detailed shape of the favoured spikes will depend sharply on K_{Gu}/G. When the other parameters are kept constant, the base of the favoured spike shape generally increases as K_{Gu}/G increases. The lipid bilayer bending resistance does not favour a small radius of curvature at the top and at the base of the spikes.

The range of geometrics of blebb-shaped protrusions which satisfied a selected cell volume and surface area generally turned out to be very limited. These cell shapes were therefore not analysed further.

Invaginated cell shapes

The invaginated cell shapes generated by the class IV parameterization (Fig. 1D) consist of N identical segments each containing one N-th of the total cell volume, cell lipids, and spectrin network. Each segment has a local axis of rotational symmetry and contains one pointed or blebb-shaped membrane invagination. The justification for using this cell shape approximation is the same as for class III cell shapes.

Figure 10 shows $\Delta F_1' = I_1' + (K_{Gu}/G)\, I_3'$, I_4', and $\partial A_d'/\partial z'$ for a cell with 32 identical invaginations and $\xi_d = 0.7$. Except for the trilayer couple term the

various terms of the invaginated cell shape show the same general trends as for crenated cells. The invaginations of the favoured invaginated cell shape are predicted to increase in number and become more pointed as Π_{Gu} becomes more positive when Π_{Eu} and Π_{Pu} have the same sign. The maximum spectrin gel density is predicted to be at the bottom of the invaginations (Fig. 10A inset). The general features are qualitatively the same for pointed and blebb-shaped invaginations.

Erythrocyte cell shape class diagram

For given shape Ψ_u and values for ξ_d, K_{Gu}/G, $B_L/(GR_0^2)$, Π_{Gu}/G, Π_{Eu}/Π_{Pu}, K_{Lu}/G, a', and b' the favoured cell shape *within* a shape class is the one which corresponds to the lowest value of the elastic free energy $\Delta F'_{\text{tot}}$. To determine the favoured cell shape class for a given set of conditions one should compare the values for the lowest $\Delta F'_{\text{tot}}$ within each class with one another. The cell shape class with the lowest $\Delta F'_{\text{tot}}$ minimum will be the class that contains the stable cell shape. The other shape classes may contain metastable shapes.

The favoured discocyte and stomatocyte shapes for two different cell volumes and various Ψ_u are shown in Fig. 11. The stable shape for each volume and Ψ_u is depicted using a solid line, the broken line depicts a metastable shape. The value of $\Delta F'_{\text{tot}}$ for each cell shape is given. Since the favoured discocyte and stomatocyte shapes are separated by intermediate shapes with higher energy, we conclude that the favoured shape within one of the shape classes is stable whereas the favoured shape within the other shape class is metastable. The free energy difference between the favoured discocyte and stomatocyte shape is particularly small, suggesting that discocytes and stomatocytes are likely to coexist. When Π_{Eu} and Π_{Pu} have the same sign, large negative Π_{Gu} favours echinocytes whereas large positive Π_{Gu} favours invaginated cell shapes. This can be summarized in an erythrocyte cell shape class diagram showing the stable shape class for any given Π_{Gu} and ξ_d (Fig. 12).

The precise location of the boundaries of the stable region of cell shape class III and IV depends mainly on K_{Gu}/G. The smaller K_{Gu}/G is, the smaller is the magnitude of $(\Pi_{Gu}/G)\,d'$ needed to include a cell shape transition. When $K_{Gu}/G = \infty$, $B_L/(GR_0^2) = 10^{-4}$ and $d' = 10^{-3}$, the transitions occur for $\Pi_{Gu} \approx 20\,G \approx 0.2$ dyne/cm and $\Pi_{Gu} \approx -100\,G \approx -1$ dyne/cm, the exact value depending on ξ_d. When $K_{Gu}/G = 1$ the transitions occur at approximately half these values of Π_{Gu}. Using known molecular parameters for the spectrin membrane skeleton and

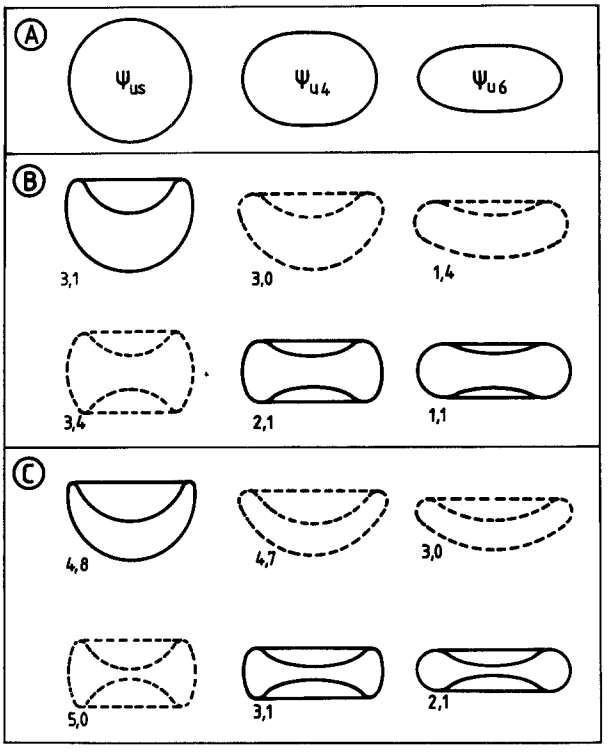

Fig. 11. Cross-section through the axis of rotational symmetry for Ψ_{u5}, Ψ_{u4} and Ψ_{u6} (**A**). Calculated stable (——) and metastable (– – – –) cell shapes when $\Pi_{Gu} = \Pi_{Eu} = \Pi_{Pu} = 0$ for $\Psi_u = \Psi_{u5}$ and various $\Psi_u = \Psi_{un}$. The number associated with each shape is the elastic free energy ($\Delta F'_{\text{tot}}$) times 1,000. The elastic free energy and the shape were determined for relaxed spectrin gel, $K_{Gu}/G = 1.0$, $B_L/(GR_0^2) = 10^{-4}$, and $\xi_d = 0.7$ (**B**) and $\xi_d = 0.5$ (**C**)

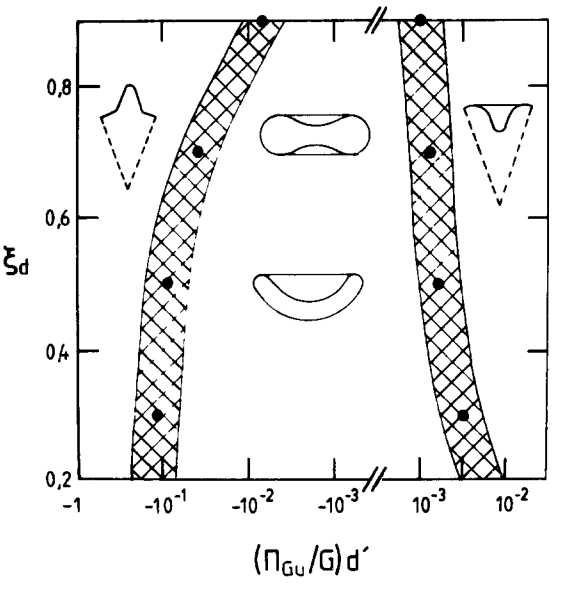

Fig. 12. A cell shape class diagram showing the stable cell shape class for various values of ξ_d and $(\Pi_{Gu}/G)\,d'$ when $K_{Gu}/G = 1.0$

assuming that the membrane skeleton constitutes a two dimensional gel, our calculations (Stokke et al. 1986) suggest that Π_{Gu} may easily range from -1 dyne/cm to $+2$ dyne/cm as the result of changing $\Delta F_c/(\mathrm{kT})$ (ΔF_c is the chain-chain affinity) and g (the number of effective dissociated hydrogen ions per gel chain). These calculated tensions Π_{Gu} needed to induce erythrocyte shape transformations are consistent with the observation that lipid bilayers can generally sustain tension down to about -100 dyne/cm (Papahadjopoulos 1968) and up to about $+(3-4)$ dyne/cm (Kwok and Evans 1981) and still maintain their normal structure.

We find that the differences between the free energy of discocytes and stomatocytes are generally so small that a large number of freely variable parameters is needed in the shape parameterizations in order to predict the precise location of the boundaries. We have therefore only indicated that there may be a region of coexistence between shape class I and II for low values of $(\Pi_{Gu}/G)\,d'$.

Stokke et al. (1986) show that when $\Delta F_c/(\mathrm{kT}) \geq 5$ small values of g correspond to negative values of Π_{Gu}. Reduction of pH towards the isoelectric point of spectrin can therefore be expexted to give rise to negative values of Π_{Gu} and thus crenation (class III cells). The observation that reduction of pH from 7.4 to 5.5 induces crenation of erythrocyte ghosts (Nicolson 1973) is consistent with this prediction because the isoelectric point of spectrin is about 4.8 (Elgsaeter et al. 1976). However, note that reduction of g may also lead to reduction of K_{Gu} and thereby induce shape transformation. The effective value of g further depends on the ionic composition of the buffer in which the membranes are located. Experimental and theoretical studies show that divalent cations are much more efficient in reducing g than monovalent cations (Tanaka et al. 1980). In agreement with this Johnson and Robinson (1976) found that the presence of 1 mM $CaCl_2$, $MgCl_2$, or $SrCl_2$ would cause crenation of ghosts whereas 100 mM KCl or NaCl was needed to obtain the same effect. Elgsaeter et al. (1976) found that the presence of more than 2 mM $CaCl_2$ induced extrusion of large spectrin and intramembrane particle free lipid vesicles from erythrocyte ghosts. This may, as suggested by the authors, come about because Π_{Gu} for these Ca^{++}-concentrations exceeds the critical value for membrane lipid bilayer collapse. Elgsaeter and Branton (1974) found that increase of the NaCl concentration to more than about 100 mM gave rise to intramembrane particle aggregation in ghosts where the spectrin network was partly broken down. This can be interpreted as a manifestation of increased negative osmotic tension in the gel as a result of the increase in the NaCl concentration. Our calculations (Stokke et al. 1986) show that large values of g can give rise to the high positive values of Π_{Gu} which favour membrane invaginations (Fig. 11). For a spectrin network, high pH and low ionic strength (Elgsaeter et al. 1976) yield a large value of g. But, because high pH and low ionic strength are also the conditions that lead to spectrin release from the membrane (Elgsaeter and Branton 1974), these conditions might be expected to cause membrane breakdown at the same time as they cause membrane invagination. High pH and low ionic strength are indeed the conditions used to form inside-out membrane vesicles (Steck et al. 1970).

Any asymmetric changes in the lipid composition of the two halves of the membrane lipid bilayer can be expected to give rise to a change in Π_{Eu}/Π_{Pu} and thus parameter d' in Eq. (1). Asymmetric incorporation of drugs can be expected to have the same effect. The membrane model therefore also offers a molecular basis for the shape transformations observed if amphiphatic drugs or phosphorylated lipids are asymmetrically incorporated into the membrane or if there is an asymmetric enzymatic breakdown of the membrane lipid bilayer (Sheetz and Singer 1974; Fairbanks et al. 1981; Tamura and Fujii 1981). The parameter d' may also depend on the ionic strength because Π_{Eu}/Π_{Pu} may change both as a result of charge effects within the lipid monolayers (Papahadjopoulos 1968) and the extracellular glycoproteins (Doulah et al. 1984).

Not only g, but also ΔF_c can be expected to change as the result of changes in the pH and ionic composition of the medium surrounding the membrane. ΔF_c may also change as a result of changes in the membrane lipid composition. The change in cell shape in response to a gradual variation in a single environmental parameter can therefore be quite complex.

Lange et al. (1982a, b) concluded that the crenatability of standard ghosts is fostered by a shift of material between the two halves of the membrane lipid bilayer during erythrocyte lysis. The protein gel – lipid bilayer membrane model offers a simple molecular basis for how such a shift in material can give rise to change in crenatability. Lange et al. (1982a) further observed that the isolated spectrin shells of crenated ghosts were smooth and concluded from this that the lipid bilayer and not the spectrin network is responsible for crenation. The protein gel – lipid bilayer membrane model shows how erythrocytes with a smooth spectrin shell can become crenated and predicts that neither the lipid nor the spectrin network, but the lipid bilayer and the spectrin network *together* are responsible for crenation.

Concluding remarks

Our numerical analysis of human erythrocyte shape using the protein gel – lipid bilayer membrane model shows that all the commonly observed erythrocyte shape classes can be accounted for by the new model. The free energy difference between discocytes and stomatocytes is found to be relatively small and which shape class is favoured depends critically on factors such as Ψ_u and the relative cell volume, ξ_d. Because of the small difference in the energy between these two shape classes they may often coexist; which shape class is the stable one can be expected to vary in response to minor changes in Ψ_u or in the environmental conditions. Crenated cell shapes are favoured by large negative values of Π_{Gu} and invaginated cell shapes by large positive values of Π_{Gu}. Our analysis give numerical estimates of the values of Π_{Gu} required to favour either crenated or invaginated cell shapes. These numerical values are well within the range that can feasibly be sustained by a lipid bilayer. Our analysis further shows that the large change in K_{Gu} predicted to occur in response to environmental changes can give rise to cell shape transformations, as well as cell shape changes within the same cell shape class. The membrane model also accounts for how changes in the membrane lipid may give rise to cell shape changes and shape transformations.

Acknowledgements. We gratefully acknowledge the continued interest and encouragements of Dr. Daniel Branton throughout this study. The study was partly supported by a grant from Norges tekniske høgskoles fond to B.T.S. We thank RUNIT Computing Centre at The University of Trondheim for allowing us to carry out most of the numerical analysis free of charge.

References

Bennet V (1982) The molecular basis for membrane – cytoskeleton association in human erythrocytes. J Cell Biochem 18:49–65

Brailsford JD, Bull BS (1973) The red cell. A macromodel simulating the hypotonic – sphere isotonic – disc transformation. J Theor Biol 39:325–332

Brailsford JD, Korpman RA, Bull BS (1976) The red cell shape from discocyte to hypotonic spherocyte. A mathematical delineation based on a uniform shell hypothesis. J Theor Biol 60:131–145

Brailsford JD, Korpman RA, Bull BS (1980a) Crenation and cupping of the red cell: A new theoretical approach. Part I. Crenation. J Theor Biol 86:513–529

Brailsford JD, Korpman RA, Bull BS (1980b) Crenation and cupping of the red cell: A new theoretical approach. Part II. Cupping. J Theor Biol 86:531–546

Branton D, Cohen CM, Tyler J (1981) Interaction of cytoskeletal proteins on the human erythrocyte membrane. Cell 24:24–32

Bull B (1972) The red cell biconcavity and deformability. A macromodel based on flow chamber observations. Nouv Rev Fr Hematol 12:835–844

Canham PB (1970) The minimum energy of bending as a possible explanation of the biconcave shape of the human red blood cell. J Theor Biol 26:61–81

Cohen CM (1983) The molecular organization of the red cell membrane skeleton. Semin Hematol 20:141–158

Deuling HJ, Helfrich W (1976) Red blood cell shapes as explained on the basis of curvature elasticity. Biophys J 16: 861–868

Doulah FA, Coakley WT, Tilley D (1984) Intrinsic electric fields and membrane bending. J Biol Phys 12:44–51

Elgsaeter A, Branton D (1974) Intramembrane particle aggregation in erythrocyte ghosts I. The effects of protein removal. J Cell Biol 63:1018–1030

Elgsaeter A, Shotton DM, Branton D (1976) Intramembrane particle aggregation in erythrocyte ghosts II. The influence of spectrin aggregation. Biochim Biophys Acta 426: 101–122

Evans EA (1973) New membrane concept applied to the analysis of fluid shear- and micropipette-deformed red blood cells. Biophys J 13:941–954

Evans EA (1974) Bending resistance and chemically induced moments in membrane bilayers. Biophys J 14:923–931

Evans EA, Hochmuth RM (1977) A solid – liquid composite model of the red cell membrane. J Membr Biol 30: 351–362

Evans EA, Hochmuth RM (1978) Mechanochemical properties of membranes. Curr Top Membr Transport 10:1–64

Evans EA, Skalak R (1979) Mechanics and thermodynamics of biomembranes. Crit Rev Bioeng 3:181–420

Fairbanks G, Patel VP, Dino JE (1981) Biochemistry of ATP-dependent red cell membrane shape change. Scand J Clin Lab Invest 41:139–144

Fung YCB, Tong P (1968) Theory of the sphering of red blood cells. Biophys J 8:175–198

Gratzer WB (1983) The cytoskeleton of the red blood cell. Stracher A (ed) Muscle and nonmuscle motility. Academic Press, New York, pp 37–124

Johnson RM, Robinson J (1976) Morphological changes in asymmetric erythrocyte membranes induced by electrolytes. Biochem Biophys Res Commun 70:925–931

Kwok R, Evans E (1981) Thermoelasticity of large lecithin bilayer vesicles. Biophys J 35:637–652

Lange Y, Hadesman RA, Steck TL (1982a) Role of the reticulum in the stability and shape of the isolated human erythrocyte membrane. J Cell Biol 92:714–721

Lange Y, Gough A, Steck TL (1982b) Role of the bilayer in the shape of the isolated erythrocyte membrane. J Membr Biol 69:113–123

Markin VS (1981) Lateral organization of membranes and cell shape. Biophys J 36:1–19

Nicolson GL (1973) Anionic sites of human erythrocyte membranes I. Effects of trypsin, phospholipase C, and pH on the topography of bound positively changed colloidal particles. J Cell Biol 57:373–389

Papahadjopoulos D (1968) Surface properties of acidic phospholipids: Interaction of monolayers and hydrated liquid crystals with uni- and bivalent metal ions. Biochim Biophys Acta 163:240–254

Sheetz MP (1983) Membrane skeletal dynamics: Role in modulation of red cell deformability, mobility of transmembrane proteins, and shape. Sem Hematol 20:175–188

Sheetz MP, Singer SJ (1974) Biological membranes as bilayer couples. A molecular mechanism of drug-erythrocyte interactions. Proc Natl Acad Sci USA 71:4457–4461

Sheetz MP, Painter RG, Singer SJ (1976) Biological membranes as bilayer couples. III. Compensatory shape changes induced in membranes. J Cell Biol 70:193–203

Skalak R, Tozeren A, Zarda RP, Chien S (1973) Strain energy function of red blood cell membranes. Biophys J 13: 245–264

Steck TL, Weinstein RS, Straus JH, Wallach DFH (1970) Inside-out red cell membrane vesicles: Preparation and purification. Science 168:255–257

Stokke BT (1985) The role of spectrin in determining mechanical properties, shapes, and shape transformations of human erythrocytes. Dr. ing. thesis, University of Trondheim, 4.34–4.52

Stokke BT, Mikkelsen A, Elgsaeter A (1986) The human erythrocyte membrane skeleton may be an ionic gel. I. Membrane mechanical properties. Eur Biophys J 13: 203–218

Tamura A, Fujii T (1981) Roles of charged groups on the surface of membrane lipid bilayer of human erythrocytes in induction of shape change. J Biochem 90:629–634

Tanaka T, Filmore D, Sun ST, Nishio I, Swislow G, Shah A (1980) Phase transitions in ionic gels. Phys Rev Lett 45: 1636–1639